Multi-aliquot method for determining (U+Th)/He ages of hydrothermal hematite: Returning to Elba

Li-Yan Wu[a *], Finlay M. Stuart[b], Luigia Di Nicola[b], Matthew Heizler[c], Marco Benvenuti[d] and Rui-Zhong Hu[a,e]

[a] State Key Laboratory of Ore Deposit Geochemistry, Institute of Geochemistry, Chinese Academy of Sciences, Guiyang 550002, China

[b] Isotope Geosciences Unit, Scottish Universities Environmental Research Centre, Rankine Avenue, East Kilbride, G75 0QF, UK

[c] New Mexico Bureau of Geology, Socorro NM 87801, USA

[d] Department of Earth Sciences, University of Florence, 50121 Florence, Italy

[e] College of Earth and Planetary Sciences, University of Chinese Academy of Sciences, Beijing 100049, China

[*]Corresponding author: wuly1982@163.com (L.Y. Wu).

Abstract

We have used a multi-aliquot method to obtain precise (U+Th)/He ages of hydrothermal hematite and to assess the extent to which He loss from fine-grained hematite caused by diffusion and recoil. Hematite (n=6) from the Rio Marina mine, Elba (Italy) yields (U+Th)/He ages that range from 5.36 ± 0.33 to 5.64 ± 0.11 Ma, giving a weighted mean age of 5.53 ± 0.14 Ma and an isochron age of 5.25 ± 0.20 Ma. $^{40}Ar/^{39}Ar$ data from cogenetic adularia yield flat age spectra with analytically indistinguishable plateau ages (5.575 ± 0.008 and 5.583 ± 0.013 Ma). An additional adularia has a more complex spectrum and yields an interpreted age of 5.64 ± 0.03 Ma. The hematite (U+Th)/He ages overlap the $^{40}Ar/^{39}Ar$ ages, albeit they are less precise (2-6% vs. 0.2-0.5%). This indicates that the loss of *in situ* radiogenic ^{4}He from complex fine-grained hematite, either by diffusion and recoil, is insignificant. The study shows that multi-aliquot method has the potential to reliably deliver precise and accurate ages for iron oxide mineralisation that has not suffered significant post-crystallisation thermal perturbation.

Keywords: (U+Th)/He; hematite; $^{40}Ar/^{39}Ar$; adularia; Elba

1. Introduction

The incorporation of modest amounts of U and Th (few ppm) in iron oxide minerals such as goethite, hematite and magnetite makes them candidates for (U+Th)/He dating. Early studies yielded geologically reasonable (U+Th)/He ages from Pliocene to Mesozoic hematite (Wernicke and Lippolt, 1993, 1994a, b; 1997; Lippolt et al., 1995). Systematic laboratory studies have shown that the ^{4}He closure temperature (T_c) of hematite depends on the grain size; massive hematite with grain diameters in excess of 100 μm has T_c > 200°C, while it approaches 50°C in fine-grained crystallites typical of botryoidal hematite (<1 μm) (e.g. Lippolt et al., 1993; Bähr et al., 1994; Farley and Flowers, 2012). This has been confirmed by computational methods (Balout et al., 2017).

Most (U-Th)/He dating studies of iron oxides/oxyhydroxides measure the He, U and Th in the same sub-mg-sized fragments of material (e.g. Farley and Flower, 2012; Vasconcelos et al. 2013). This technique allows dating of intergrown and fine-grained minerals and in recent years it has proved to be a powerful method for determining the timing of processes that have hitherto proved difficult, such as the timing of fault movement (e.g. Evenson et al., 2014; Ault et al., 2015; McDermott et al., 2017) and regional weathering events (Shuster et al., 2005; Cooper et al. 2016; Deng et al., 2017). However, the method is analytically challenging and has complexities that are often not evident from age data. For instance, over-heating of the iron oxides/oxy-hydroxides can result in the volatilization loss of U (and Th) leaving the resultant ages significantly younger than the crystallisation age (e.g. Vasconcelos et al.

2013; Cooper et al. 2016). Under-heating of samples can lead to the incomplete degassing of He yielding ages that are significantly younger than the crystallisation age (e.g. Danisik et al. 2013). Multiple analyses of same age material typically yield strongly (±20%) over-dispersed ages, even after rejection of obviously over-heated grains (e.g. Cooper et al. 2016).

Here we present new (U+Th)/He ages of hydrothermal hematite where ^{4}He is measured on separate aliquots of the same sample from U and Th. We revisit the seminal study of Lippolt et al. (1995) who determined (U+Th)/He ages of hydrothermal hematite and compared them to K-Ar ages of cogenetic adularia from the Miocene-aged hydrothermal mineralisation from the island of Elba, Italy. We report multi-aliquot hematite He ages and high precision adularia ^{40}Ar/^{39}Ar ages with the aim of assessing the age precision attainable using the multi-aliquot technique, and determining the extent to which diffusion and α recoil result in ^{4}He loss from hematite.

2. Sample location and description

Several iron ore deposits are present on the eastern coast of Elba between Monte Calendozio and Capo Calamita. Three major iron ore types can be distinguished on Elba Island (Tanelli et al., 2001; Dünkel, 2002): Rio Marina type (deposits of Rio Marina and Rio Albano, northeastern Elba, characterized by lenticular bodies of hematite-pyrite (+limonite)), Ortano type (including the deposits of Ortano and Terra Nera (central east), characterized by hematite-magnetite-pyrite),

78 and Calamita type (deposits of Sassineri, Ginevro and Calamita, comprising lenses
79 and massive bodies of magnetite ± hematite associated to skarn bodies in the
80 Calamita Peninsula (southeast)). The deposits were likely formed
81 contemporaneously with the shallow intrusion of the nearby Porto Azzurro quartz
82 monzonitic intrusion at 5.9 ± 0.2 Ma (Maineri et al., 2003). There is little consensus
83 on the source of the iron in the Elba deposits; it may be sedimentary in origin,
84 remobilised by hydrothermal fluids (Tanelli and Lattanzi, 1986; Dünkel, 2002) or of
85 magmatic origin (Lotti, 1929; Gillieron, 1959).

86 The ore bodies of the first type at the Rio Marina mine are typically stratiform
87 and vein-type, hosted by quartz–phyllite units of the Carboniferous-Triassic Tuscan
88 Nappe, often close to the contact with overlying carbonates. The hematite in the
89 deposits is typically lamellar/micaceous, associated with pyrite, quartz, and chlorite.
90 Iron ores from the Valle Giove stope also contain abundant adularia and have been
91 targeted in this study.

92 We have analysed vein hematite from the Valle Giove stope in the Rio Marina
93 mine district. Three samples (Italy-1, -2 and -3) are dominated by specular (micaceous)
94 hematite and contain abundant cogenetic adularia (Figure 1). Hand specimen Italy-4
95 contains both coarse- (Italy-4c) and fine-grained (4f) micaceous hematite. Sample
96 M1392 is a massive (oligistic) hematite mostly formed of flattened rhombohedrons
97 that are up to 2 cm long. Hematites from Italy-1 to -4 are generally comprised of
98 aggregates of plate-shaped crystals that are 20-5 μm thick (Figure 2A and B). The
99 oligistic hematite of M1392 is poly-crystalline, comprised of less well-ordered

hematite plates that are significantly thinner that the micaceous hematites (Figure 2C). All hematites are compositionally homogeneous and there is no evidence of mineral inclusions or recrystallisation/zonation (not shown). Back-scattered electron (BSE) and electron microprobe element mapping of adularias show that they are homogeneous and contain no significant Ca (Figure 2 G-U). This is consistent with the Ar/Ar data (Table 2). There is no indication of multiple generations of adularia growth nor significant sericite alteration.

3. Analytical procedures

3.1 Hematite (U+Th)/^{4}He dating

The analytical procedure reported here differs from the majority of previous studies that measure He, U and Th concentrations on the same aliquot of hematite. In this study we have measured He and U-Th in separate aliquots of hematite from the same sample. This avoids the problem of incomplete He extraction and U volatilization due to under- and over-heating respectively, though it requires significantly more laboratory effort and the availability of larger sample mass (Farley and McKeon, 2015).

Several grams of hematite were carefully removed from each sample to minimize the incorporation of gangue minerals. The hematite fragments were crushed and any visible gangue minerals removed from the 100-200 μm fraction by handpicking under a binocular microscope. The handpicked separate was then gently crushed and fully mixed.

Aliquots of 10-20 mg of ~30 μg grains were weighed into 10 x 2.5 mm Pt-foil tubes. The tubes were crimped at both ends then placed into recesses in a fully degassed Cu pan then pumped to $<10^{-8}$ torr prior to degassing at 80°C for 3 hours. Helium was extracted by heating each packet to ~1300°C for 10 minutes by rastering a diode laser beam along the length of the tube. The temperature of the packet was assessed by visual observation of the color emitted from heated Pt tubes. A sapphire cover glass was used to avoid volatilized metal from absorbing onto the sapphire viewport. The liberated gases were purified by exposure to two liquid nitrogen-cooled charcoal traps during heating and for a further 15 minutes. ^{4}He abundances along with H (mass 2) and CH_4 (mass 16) were determined by an electron multiplier in a Hiden HAL3F quadrupole mass spectrometer operated in static mode following procedures in Foeken et al. (2006). Absolute He concentrations were calculated by peak height comparison against a calibrated He standard. The precision of He measurements was determined by repeated measurements of the gas standard. Within-day reproducibility of measurement of the ^{4}He standard was typically ±0.4% (2σ, n = 10-12). Laser heating of empty Pt tubes yielded He levels (1.6×10^{-11} ml, n = 9) that were close to system background levels. To verify complete extraction of He each sample was re-heated to 1300-1400°C for a further 10 minutes. Between three and five aliquots of each sample were measured.

U and Th concentrations were measured in three to five aliquots of hematite (3-11 mg) that had not been used for He extraction using an Agilent 7500ce

Q-ICP-MS. An initial analysis of natural U and Th in each sample was done in order to optimise the spike amount for sample/spike ratios that were between 0.1 and 10. Each sample was loaded into a Teflon beaker with a dilute-spike solution equivalent to 2-4 ng of ^{230}Th and 1-2 ng of ^{235}U in 2 ml 12 M HCl. The beakers were then heated to 100°C for 2 days to completely dissolve the iron oxide. The HCl was then evaporated off and the dried residues were refluxed with 2 ml of 1.5 M HNO_3 at 80°C overnight. Pre-cleaned columns were filled with pre-cleaned TR-B50-S resin, and washed with 9 ml of 0.2 M HCl and 9 ml of 0.1 M HCl + 0.3 M HF. The resin was pre-conditioned using 9 ml of 1.5 M HNO_3 before the sample was introduced in 2 ml 1.5 M HNO_3. Matrix elements were removed by rinsing the columns with 12 ml 1.5M HNO_3 and 2.5 ml 3 M HCl. U and Th were eluted using 12 ml mixture of 0.1 M HCl 0.3 M HF. The final elutes were evaporated to dryness on a hotplate at 80°C then set to reflux with 2 ml of 0.8M HNO_3 for 24 hours. The long-term blanks averaged 0.52 ng (n=11) for ^{238}U and 0.16 ng (n=11) for ^{232}Th. These levels were negligible in comparison to sample U and Th concentrations. The Sm content of Elba hematites have been shown by Lippolt et al. (1995) to be insignificant to the production of ^{4}He so were not determined.

3.2 Adularia ^{40}Ar/^{39}Ar dating

The ^{40}Ar/^{39}Ar age determinations were performed at the New Mexico Geochronology Research Laboratory. Adularia was hand-picked from crushed samples then irradiated at the TRIGA reactor in Denver, Colorado for 12 hours in the

NM-290 package along with Fish Canyon Sanidine interlaboratory standard FC-2 with an assigned age of 28.201 Ma (Kuiper et al., 2008). Ages are calculated with a total ^{40}K decay constant of 5.463 x 10^{-10} a^{-1} (Min et al., 2000).

After irradiation, six crystals of FC-2 from each of 8 monitor holes from a 24-hole irradiation tray, along with ~1 mg sample aliquots were loaded into a copper tray, evacuated and baked at 140°C for 2 hours. FC-2 crystals were fused and adularia was step-heated both with a CO_2 laser and the extracted gas was cleaned with a SAES NP10 getter operated at 1.6 A and a D50 getter at 20°C for 30 seconds. The gas was analyzed for argon isotopes using a ThermoScientific ARGUS VI multi-collector mass spectrometer equipped with five Faraday cups, and one ion counting multiplier (CDD). The configuration had ^{40}Ar, ^{39}Ar, ^{38}Ar, ^{37}Ar and ^{36}Ar on the H1, AX, L1, L2, and CDD detectors, respectively. H1, AX and L2 utilized Faraday detectors equipped with 10^{13} Ω resistors whereas L1 had a Faraday with a 10^{14} Ω resistor. The CDD is an ion counting detector with a dead time of 14 ns. All data acquisition was accomplished with NM Tech Pychron software and data reduction used Mass Spec (v.7.875) written by Al Deino at the Berkeley Geochronology Laboratory. Extraction line blank plus mass spectrometer background values are averages of numerous measurements interspersed with the unknown measurements. These values are 12 ± 4%, 0.2 ± 9%, 0.08 ± 10%, 0.4 ± 3%, 0.06 ± 6%, x 10^{-17} moles for masses 40, 39, 38, 37, and 36, respectively.

Plateau ages are calculated for the indicated steps and represents the inverse variance weighted mean age and the error is the square root of the sum of $1/\sigma^2$

188 values. The error is also multiplied by the square root of the MSWD for MSWD
189 greater than 1. J-error (0.03%) is included for the plateau age error and all errors are
190 reported at 2σ.
191
192 **4. Results**
193 Hematite ^{4}He concentrations range from 1.39 to 17.1 x 10^{-10} ml/mg and the
194 multiple aliquots usually differ by less than 3% in each sample (Table 1). ^{238}U
195 concentrations range from 4.6 to 66.1 x 10^{11} atoms/mg and ^{232}Th concentrations range
196 from 0.1 to 13.7 x 10^{11} atoms/mg. Within-sample U concentrations vary by 3-5%.
197 Variations for ^{232}Th are larger, though the low concentrations and low production
198 ratio of ^{4}He relative to U mean that this has a rather minor effect on ages. U/Th ratios
199 of the individual aliquots range from 0.8 to 19.7 (Table 1). The within-sample
200 consistency of U/Th ratios, and the lack of variation in He, U and Th concentration in
201 multiple aliquots suggest that the crushed hematite has been adequately homogenized.
202 (U+Th)/He ages calculated using the average He, U and Th concentrations for
203 each sample range from 5.36 to 5.64 Ma (Figure 3; Table 1). The uncertainty of the
204 He ages calculated using the standard deviation of the average He and U (+Th)
205 concentrations, ranges from 2 to 6%. Uncertainties in the average He and U (+Th)
206 concentrations make approximately equal contributions to the age uncertainty.
207 Two of the three adularia samples (Italy-1 and 3) yield essentially flat $^{40}Ar/^{39}Ar$
208 age spectra giving plateau ages of 5.575 ± 0.008 and 5.583 ± 0.013 Ma (Figure 4a, c;
209 Table 2). Significant parts of these spectra that yield greater than 50% of the total ^{39}Ar

210 released have steps concordant at 2σ. For instance, steps C-K of Italy-1 containing 60%
211 of the spectrum yields an age of 5.568 ± 0.009 Ma and for Italy-3 steps E-K (68% of
212 the spectrum) yield an age of 5.574 ± 0.009 Ma. Based on the criteria for Fleck et al.
213 (1977) these ages could be argued to be the preferred ages, but we choose to include
214 the entire data set despite the very minor discordance and the fact that the overall
215 interpretation of the data are not altered by choosing subsets of the data. Several
216 features of the Ar/Ar data indicate that they provide a robust age for adularia
217 deposition. The nearly flat age spectra indicate simple argon systematics and suggest
218 that they record no significant Ar-loss during protracted cooling. Additionally, the
219 nearly undetectable ^{37}Ar signal indicates that the samples are essentially devoid of Ca
220 and the ^{39}Ar intensity coupled with sample weight and J-factor indicate K_2O contents
221 of greater than 16 weight percent. Both are indicative of pure adularia. Microprobe
222 analyses also confirm that the samples are pure adularia (Figure 2H). In contrast to
223 Italy-1 and Italy-3, Italy-2 has a more complex $^{40}Ar/^{39}Ar$ spectrum with initially old
224 ages stepping down to a minimum segment that has a weighted mean age of 5.64 ±
225 0.03 (Figure 4b). We suggest that this sample maybe contaminated with excess ^{40}Ar
226 and the age can be treated as a maximum. There is no simple isochron array, however
227 initially old steps in the age spectrum correlate to lower radiogenic yields that could
228 support and excess argon component. The lack of a well-defined isochron likely
229 suggests that both excess argon component and an atmospheric component are not
230 thermally distinct and thus record mixing between multiple sources with different
231 initial $^{40}Ar/^{36}Ar$ ratios (cf. Heizler et al., 1988).

Maineri et al. (2003) dated a magmatic muscovite, a hydrothermal sericite and a partly chloritized biotite from the region and obtained overall complex results. They concluded that complexity of the muscovite and sericite was related to mixing of variable amounts of the two phases that have discordant ages and variable Cl concentrations. They provided no explanation of the biotite age spectrum discordance and suggested that variable K/Ca values were related to Ca-rich impurities. They utilized the Cl/K (i.e. $^{38}Ar_{Cl}$/ $^{39}Ar_{K}$) data to help constrain the mixing of younger sericite with the older muscovite and concluded that sericite alteration occurred at ~6.7 Ma. Cl/K spectra (Figure 4) suggest that values are highest (>0.005) in the initial heating steps and fall to values that vary between 0.0001 and 0.0005. There is no simple correlation between Cl/K and age which further supports variable trapped initial $^{40}Ar/^{36}Ar$ components to explain the complexity of Italy-2. Therefore, unlike the complex results of Maineri et al. (2003), the adularia data are straightforward (especially Italy-1 and 3) to interpret and indicate hydrothermal precipitation of pure adularia well after an earlier sericite alteration event.

5. Discussion: Accuracy and precision of multi-aliquot (U+Th)/He ages

The new (U+Th)/He ages of the Rio Marina hematite samples overlap within uncertainty. They display significantly less variation than the age range determined in the previous study (4.8 to 7.3 Ma; Lippolt et al. 1995) (Figure 3). This is unlikely to reflect variation in the timing of hematite mineralization of the Rio Marina deposit that was not sampled in this study as the quartz monzonitic intrusion which

drove the hydrothermal system provides an upper limit to the age of mineralisation (5.9 ± 0.2 Ma; Maineri et al, 2003). The uncertainty on these hematite ages (3-5 %) is an improvement on the 10-30% age range that can result from multiple single aliquot measurements even after rejection of data affected by over-heating or inclusions (e.g. Cooper et al. 2016). This conclusion has, however, to be tempered by the recognition that the multi-aliquot technique requires significantly more sample material and analytical effort (e.g. column chemistry).

The mean (U+Th)/He age of the three hematite samples with co-existing adularia (5.56 ± 0.15 Ma) overlaps the plateau ages of the adularia with the nearly flat age spectra. This hematite age is slightly younger than the maximum $^{40}Ar/^{39}Ar$ age determined for the Italy-2 adularia, however Italy-2 likely contains excess argon based on its overall saddle-shaped age spectrum.

The mean (U+Th)/He age of all five Rio Marina hematite samples (5.53 ± 0.14 Ma) is indistinguishable from the age of the three that contain coexisting adularia, consistent with all samples originating from the same hydrothermal event. In this case the data can be used to plot an isochron (Figure 5). The isochron slope is equivalent to an age of 5.25 ± 0.20 Ma. The isochron intersects the origin within uncertainty, indicating that the hematite does not contain significant parentless ^{4}He, such as would be present in hydrothermal fluid inclusions (e.g. Stuart et al., 1995).

The similarity of the multi-aliquot hematite (U+Th)/He ages and Ar/Ar ages is strong evidence that there has been no ^{4}He loss since mineralization that can be distinguished within analytical uncertainty. This implies that diffusive loss during

post-mineralisation cooling or re-heating during subsequent hydrothermal events, and α-ejection to grain boundaries can be ignored in these samples. This is supported by the observation that the coarse and fine fractions of Italy-4 hematite yield ages that are indistinguishable within uncertainty (Table 1).

Dünkel (2002) estimate that the Rio Marina hematite precipitated at 300-320°C based on fluid inclusion homogenization temperatures in cogenetic quartz. At this temperature hematite is expected to retain no ^{4}He. The closure temperature of the Elba hematites likely range from 80 to 200°C (Lippolt et al. 1993; Bähr et al. 1994; Balout et al., 2017; Farley 2018). The similarity of the (U+Th)/He and ^{40}Ar/^{39}Ar ages of the samples is consistent with rapid cooling to <50°C after precipitation and the absence of significant re-heating.

It also implies that recoil of α particles to hematite grain boundaries does not result in the loss of significant proportion of the ^{4}He from the 10-30 μm fragments analysed in this study. This may be a consequence of the grain boundaries being volumetrically insignificant, or that they do not form a connected network that promotes the loss of He from intergrown sub-μm hematite crystallites.

6. Conclusion

(U+Th)/He ages have been determined from several fine-grained vein hematite samples from Rio Marina mine, Elba, using a multiple aliquot technique. The low variability in He and U concentrations in 3-5 aliquots from each sample suggests that crushing to <30 μm is adequate to homogenise 5-10 mg of hematite in this case. The

298 data define a coherent isochron consistent with an absence of parentless ^{4}He (e.g. in
299 hydrothermal fluid inclusions) in the hematite. The new He ages overlap high
300 precision $^{40}Ar/^{39}Ar$ age of coexisting adularia which implies that diffusion and recoil
301 loss of ^{4}He from hematite microcrysts are not significant, and that the He ages record
302 the time of mineralisation. The multi-aliquot technique avoids the analytical
303 challenges associated with techniques where He, U and Th are measured on the same
304 aliquot, and demonstrates that the method has the potential to reliably deliver precise
305 and accurate ages for iron oxide precipitation that has not suffered significant
306 post-crystallisation thermal perturbation. The coherence of the hematite-adularia ages,
307 and the apparent homogeneity of He, U and Th (at the sample mass analysed here)
308 suggests that Elba hematite may prove a useful secondary mineral standard analogous
309 to the Durango apatite for (U+Th)/He dating.

310 The $^{40}Ar/^{39}Ar$ ages of the Rio Marina mine adularia are the first high precision
311 ages of the Elba iron oxide mineralization. The ages overlap the K-Ar age for the
312 Porto Azzurro monzonite (5.9 ± 0.2 Ma; Maineri et al., 2003) confirming the genetic
313 link. Further they provide a baseline for future chronology studies aimed at
314 determining the history of iron mineralization on Elba.

315

316 **Acknowledgements**

317 This work was financially supported by SUERC, the National Key Research and
318 Development Program of China (2016YFC0600207), the Strategic Priority Research
319 Program (B) of Chinese Academy of Sciences (XDB18000000) and National Natural

Science Foundation of China (41773048). We thank two journal reviewers for comments that improved this work.

References

Ault, A.K., Reiners, P.W., Evans, J.P., and Thomson, S.N., 2015. Linking hematite (U–Th)/He dating with the micro-textural record of seismicity in the Wasatch fault damage zone, Utah, USA. Geology, 43(9): 771–774.

Bähr, R., Lippolt, H.J. and Wernicke, R.S., 1994. Temperature–induced ^{4}He degassing of specularite and botryoidal hematite: A ^{4}He retentivity study. Journal of Geophysical Research, 99(89): 17695–17707.

Balout, H., Roques, J., Gautheron, C., Tassan–Got, L. and Mbongo–Djimbi, D., 2017. Helium diffusion in pure hematite (α–Fe_2O_3) for thermochronometric applications: A theoretical multi–scale study. Computational and Theoretical Chemistry, 1099: 21–28.

Cooper, F.J., Adams, B.A., Blundy, J.D., Farley, K.A., McKeon, R.E., Ruggiero, A. 2016. Aridity-induced Miocene canyon incision in the Central Andes. Geology, 44: 675–678.

Danišík, M., Evans, N.J., Ranmanaidou, E., McDonald, B.J., Mayers, C. and McInnes, B.I.A., 2013. (U–Th)/He chronology of the Robe River channel iron deposits, Hamersley Province, Western Australia. Chemical Geology, 354: 150–162.

Deng, X.D., Li, J.W. and Shuster, D.L., 2017. Late Mio-Pliocene chemical weathering of the Yulong porphyry Cu deposit in the eastern Tibetan Plateau constrained by

342 goethite (U–Th)/He dating: Implication for Asian summer monsoon. Earth and
343 Planetary Science Letters, 472: 289–298.
344 Dünkel, I., 2002. The genesis of East Elba iron ore deposits and their interrelation
345 with Messinian tectonics. PhD, University Tuebingen, A65, 1–143.
346 Evenson, N.S., Reiners, P.W., Spencer, J.E. and Shuster, D.L., 2014. Hematite and
347 Mn oxide (U–Th)/He dates from the Buckskin–Rawhide detachment system,
348 western Arizona: Gaining insights into hematite (U–Th)/He systematics. American
349 Journal of Science, 314(10): 1373–1435.
350 Farley, K.A., 2018. Helium diffusion parameters of hematite from a single-diffusion
351 -domain crystal. Geochimica et Cosmochimica Acta, 231: 117–129.
352 Farley, K.A. and Flowers, R.M., 2012. (U–Th)/Ne and multi-domain (U–Th)/He
353 systematics of a hydrothermal hematite from eastern Grand Canyon. Earth and
354 Planetary Science Letters, 359–360: 131–140.
355 Farley, K.A. and R. McKeon, R., 2015. Radiometric dating and temperature history of
356 banded iron formation–associated hematite, Gogebic iron range, Michigan, USA.
357 Geology 34; 1083-1086.
358 Fleck, R.J., Sutter, J.F., and Elliot, D.H., 1977, Interpretation of discordant $^{40}Ar/^{39}Ar$
359 age-specta of Mesozoic tholeiites from Antarctica. Geochimica et Cosmochimica
360 Acta, 41: 15–32.
361 Foeken, J.P.T., Stuart, F.M., Dobson, K.J., Persano, C.P., and Vilbert, D., 2006, A
362 diode laser system for heating minerals for (U-Th)/He chronometry: Geochemistry,
363 Geophysics, Geosystems, 7(4), DOI: 10.1029/2005GC001190.

364 Gillieron, F., 1959. Osservazioni sulla geologia dei giacimenti di ferro dell'Elba
365 orientale. L'Industria Mineraria, 10: 1–10.
366 Heizler, M.T. and Harrison, T.M., 1988, Multiple trapped argon isotopic components
367 revealed by $^{40}Ar/^{39}Ar$ isochron analysis. Geochimica et Cosmochimica Acta, 52:
368 295–1303.
369 Kuiper, K.F., Deino, A., Hilgen, F.J., Krijgsman, W., Renne, P.R., and Wijbrans, J.R.,
370 2008, Synchronizing rock clocks of Earth history: Science, 25: 500–504.
371 Lippolt, H.J., Wernicke, R.S. and Boschmann, W., 1993. ^{4}He diffusion in specular
372 hematite. Physics and Chemistry of Minerals, 20(6): 415–418.
373 Lippolt, H.J., Wernicke, R.S. and Bähr, R., 1995. Paragenetic specularite and adularia
374 (Elba, Italy): Concordant (U+Th)–He and K–Ar ages. Earth and Planetary Science
375 Letters, 132: 43–51.
376 Lotti, B., 1929. I depositi dei minerali metalliferi. Edizioni L'Industria Mineraria,
377 Genova, 236 p.
378 Maineri, C., Benvenuti, M., Costagliola, P., Dini, A., Lattanzi, P., Ruggieri, G., Villa
379 I.M., 2003. Sericitic alteration at the La Crocetta deposit (Elba Island, Italy):
380 interplay between magmatism, tectonics and hydrothermal activity. Mineralium
381 Deposita, 38: 67–86.
382 McDermott, R.G., Ault, A.K., Evans, J.P. and Reiners, P.W., 2017.
383 Thermochronometric and textural evidence for seismicity via asperity flash heating
384 on exhumed hematite fault mirrors, Wasatch fault zone, UT, USA. Earth and
385 Planetary Science Letters, 471(1): 85–93.

386 Min, K., Mundil, R., Renne, P.R., and Ludwig, K.R., 2000. A test for systematic
387 errors in $^{40}Ar/^{39}Ar$ geochronology through comparison with U/Pb analysis of a
388 1.1-Ga rhyolite. Geochimica et Cosmochimica Acta, 64(1): 73–98.
389 Pettke, T., Frei, R., Kramers, J.D. and Villa, I.M., 1997. Isotope systematics in vein
390 gold from Brusson, Val d'Ayas (NW Italy) 3. (U + Th)He and K-Ar in native Au
391 and its fluid inclusions. Chemical Geology, 135(3): 173–187.
392 Shuster, D.L., Vasconcelos, P.M., Heim, J.A. and Farley, K.A., 2005. Weathering
393 geochronology by (U–Th)/He dating of goethite. Geochimica et Cosmochimica
394 Acta, 69(3): 659–673.
395 Steiger, R.H. and Jäger, E., 1977. Subcommission on geochronology: Convention on
396 the use of decay constants in geo- and cosmochronology. Earth and Planetary
397 Science Letters, 36, 359–362.
398 Stuart, F.M., Burnard, P.G., Taylor, R.P., Turner, G., 1995. Resolving mantle and
399 crustal contributions to ancient hydrothermal fluids: He–Ar isotopes in fluid
400 inclusions from Dae Hwa W-Mo mineralisation, South Korea. Geochimica et
401 Cosmochimica Acta, 59: 4663–4673.
402 Tanelli, G., Benvenuti, M., Costagliola, P., Dini, A., Lattanzi, P., Maineri, C.,
403 Mascaro I., Ruggieri, G., 2001. The iron mineral deposits of Elba Island: state of
404 the art. Ofioliti, 26: 239–248.
405 Tanelli, G. and Lattanzi, P., 1986. Metallogeny and mineral exploration in Tuscany:
406 state of the art. Mem. Soc. Geol. It., 31: 299–304.
407 Taylor, J.R., 1982. An introduction to error analysis: The study of uncertainties in

physical measurements, University Science Books, Mill Valley, California, 270 p.

Vasconcelos, P.M., Heim, J.A., Farley, K.A., Monteiro, H. and Waltenberg, K., 2013. $^{40}Ar/^{39}Ar$ and (U–Th)/He–$^{4}He/^{3}He$ geochronology of landscape evolution and channel iron deposit genesis at Lynn Peak, Western Australia. Geochimica et Cosmochimica Acta, 117: 283–312.

Wernicke, R.S. and Lippolt, H.J., 1993. Botryoidal hematite from the Schwarzwald (Germany): heterogeneous uranium distributions and their bearing on the helium dating method. Earth and Planetary Science Letters, 114: 287–300.

Wernicke, R.S. and Lippolt, H.J., 1994a. ^{4}He age discordance and release behavior of a double shell botryoidal hematite from the Schwarzwald, Germany. Geochimica et Cosmochimica Acta, 58(1): 421–429.

Wernicke, R.S. and Lippolt, H.J., 1994b. Dating of vein specularite using internal (U+Th)/^{4}He isochrons. Geophysical Research Letters, 21(5): 345–347.

Wernicke, R.S. and Lippolt, H.J., 1997. (U+Th)/He evidence of continuous Jurassic hydrothermal activity in the Schwarzwald basement, Germany. Chemical Geology, 138: 273–285.

York, D., 1969. Least squares fitting of a straight line with correlated errors, Earth and Planetary Science Letters, 5, 320–324.

Zuffardi, P., 1990. The iron deposits of the Elba Island (Italy): Remarks for a metallogenic discussion, Memorie Fisiche e Naturali dell'Accademia dei Lincei, 9: 99–128.

Figure captions

Figure 1. Images of hematite ore samples from San Marino mine, Elba (Italy) used in this study. (A) Italy1: micaceous specular hematite and adularia. (B) Italy2: micaceous specular hematite and euhedral adularia (1-2 mm). (C) Italy3: micaceous specular hematite and prismatic adularia. (D) M1392: massive euhedral, hematite rhombohedrons. (E) Italy4: micaceous specular hematite with coarse grained vein.

Figure 2 (A and B). Scanning electron microscope (SEM) back-scattered images of unpolished fragments of Italy-1 hematite showing the polycrystalline aggregates of plate-shaped hematite. These features are typical of all Italy-x samples. (C) SEM back-scattered image of rhombohedron hematite of M1392. The thickness of each layer of rhombohedron is probably less than 1 μm. (D-G) show back-scattered electron micoprobe and element maps of Italy-1 adularia showing homogeneous texture and lack of zonation and alteration.

Figure 2. Delete panels A, E and F. Make B new A and D new B, leave C as C. Delete all adularia figures except Italy-1.

Figure 3. Summary diagram of (U+Th)/He ages of hematite from Rio Marina mine, Elba; this work (dark circles) and Lippolt et al. (1995) (light circles). The average of the three new $^{40}Ar/^{39}Ar$ ages of cogenetic adularia (5.598 ± 0.036 Ma) is shown by the grey bar. The multi-aliquot hematite ages are more precise than those of Lippolt et al. (1995) and they overlap within uncertainty the adularia crystallisation age.

Figure 4. $^{40}Ar/^{39}Ar$ age spectra for three adularia samples from hematite mineralisation at Rio Marina, Elba. The spectra show the apparent ages, $\%^{40}Ar^*$ and Cl/K ratios measured during each heating step.

Figure 5. Isochron plot of (U + 0.232Th) vs. ^{4}He using the multi-aliquot (U-Th)/He ages of hematite from Rio Marina, Elba.

Table captions

Table 1 (U-Th)/He ages and trace element contents for several aliquots of hematite samples from Elba, Italy

Table 2 $^{40}Ar/^{39}Ar$ data of adularia cogenetic with hematite from Elba, Italy

Table 1 (U-Th)/He ages and trace element contents for several aliquots of hematite samples from Elba, Italy

Sample	Aliquot	Mass (mg)	^{4}He *	Mean ^{4}He*	Aliquot	Mass (mg)	$^{238}U^{+}$	$^{232}Th^{+}$	eU^{+}	Mean eU^{+}	He age (Ma)
Italy-1	I1He1	19.4	1.37	1.36 ± 0.01	I1U1	9.1	0.19	39	0.21	19.9 ± 0.5	5.64 ± 0.11
	I1He2	15.4	1.36		I1U2	11.9	0.19	29	0.20		
	I1He3	10.2	1.35		I1U3	7.0	0.19	23	0.20		
Italy-2	I2He1	14.3	3.93	3.81 ± 0.12	I2U1	7.1	0.56	4	0.57	58.5 ± 1.9	5.39 ± 0.23
	I2He2	13.0	3.81		I2U2	8.4	0.57	28	0.58		
	I2He3	12.0	3.68		I2U3	6.1	0.59	29	0.61		
Italy-3	I3He1	19.0	1.63	1.61 ± 0.01	I3U1	7.2	0.18	188	0.23	23.8 ± 1.0	5.59 ± 0.15
	I3He2	13.0	1.61		I3U2	6.5	0.18	238	0.24		
	I3He3	11.8	1.60		I3U3	6.3	0.19	246	0.25		
Italy-4C	I4CHe1	15.8	2.74	2.76 ± 0.02	I4CU1	8.2	0.37	450	0.47	56.5± 17	5.36 ± 0.33
	I4CHe2	12.8	2.75		I4CU2	7.4	0.63	555	0.76		
	I4CHe3	13.7	2.79		I4CU3	8.5	0.35	444	0.46		
Italy-4F	I4FHe1	20.3	3.44	3.47 ± 0.09	I4FU1	8.1	0.41	527	0.53	52.0 ±3.3	5.49 ± 0.35
	I4FHe2	18.6	3.62		I4FU2	7.7	0.42	522	0.54		
	I4FHe3	15.3	3.44		I4FU3	9.0	0.37	451	0.48		
	I4FHe4	14.4	3.36								
	I4FHe5	14.4	3.50								
M1392	MHe1	11.1	16.76	16.71 ± 0.31	MU1	8.9	2.37	142	2.42	250 ± 16	5.39 ± 0.33
	MHe2	13.2	16.22		MU2	10.2	2.61	205	2.68		
	MHe3	9.7	16.54		MU3	5.6	2.42	102	2.46		
	MHe4	9.9	17.06		MU4	5.4	2.22	78	2.25		
	MHe5	9.6	16.78		MU5	4.3	2.60	0	2.56		
					MU6	4.7	2.60	106	2.64		

* He concentrations are reported in 10^{-10} ml/mg

$^{+}$ U concentrations and mean eU+ are reported in ppm, and Th concentrations are ppb

Table 2 $^{40}Ar/^{39}Ar$ data of adularia cogenetic with hematite from Elba, Italy

ID	Power (Watts)	$^{40}Ar/^{39}Ar$	$^{38}Ar/^{39}Ar$	$^{37}Ar/^{39}Ar$	$^{36}Ar/^{39}Ar$ (x 10^{-3})	$^{39}Ar_K$ (x 10^{-15} mol)	K/Ca	Cl/K	$^{40}Ar^*$ (%)	^{39}Ar (%)	Age (Ma)	±1σ (Ma)
Italy-1, Adularia, 1.14 mg, J=0.0028246±0.01%, IC=1.00859±0.0017725, NM-290F, Lab#=65668-01, Argus VI												
C	0.3	5.591	0.0416	0.0004	15.19	2.08	1339	0.0059	19.6	1.5	5.654	0.095
D	0.4	1.830	0.0180	-0.0027	2.475	2.68	-	0.00109	59.8	3.5	5.627	0.032
E	0.4	1.613	0.0167	0.0012	1.799	3.81	411.6	0.00082	66.9	6.2	5.538	0.024
F	0.5	1.436	0.0148	0.0006	1.188	11.6	785.7	0.00042	75.4	14.7	5.556	0.011
G	0.6	1.399	0.0143	0.0011	1.053	18.3	452.4	0.00033	77.6	28.0	5.573	0.008
H	0.7	1.209	0.0136	0.0008	0.4058	14.8	624.3	0.00019	90.0	38.8	5.579	0.006
I	0.7	1.268	0.0138	0.0006	0.6189	11.9	807.2	0.00023	85.5	47.5	5.559	0.008
J	0.8	1.220	0.0138	0.0001	0.4552	17.5	6951	0.00023	88.9	60.3	5.559	0.006
K	0.9	1.291	0.0137	0.0002	0.6772	14.9	2479	0.0002	84.4	71.1	5.587	0.007
L	1.0	1.214	0.0133	-0.0003	0.4176	11.7	-	0.00012	89.8	79.6	5.585	0.007
M	1.2	1.256	0.0143	0.0005	0.5671	17.7	1031	0.00033	86.6	92.5	5.572	0.007
N	2.0	1.202	0.0141	0.0002	0.3720	10.28	2290	0.0003	90.8	100.0	5.593	0.008
Integrated age ± 2σ				n=12		137.2				K_2O=16.37%	5.574	0.008
Plateau ± 2σ	steps C-N			n=12	MSWD=2.61	137.2				100.0	5.575	0.008
Isochron±2σ	steps C-N			n=12	MSWD=3.06		$^{40}Ar/^{36}Ar$=		295.5±2.0		5.575	0.008
Italy-2, Adularia, 0.81 mg, J=0.0028247±0.01%, IC=1.00859±0.0017725, NM-290F, Lab#=65670-01, Argus VI												
C	0.3	15.87	0.0591	0.0016	48.85	1.76	322.8	0.00844	9.0	1.8	7.36	0.20
D	0.4	5.397	0.0245	0.0012	13.64	1.83	415.7	0.00209	25.2	3.7	7.006	0.081
E	0.4	2.286	0.0166	0.0039	3.531	2.22	132.0	0.00074	54.2	6.0	6.369	0.041
F	0.5	1.818	0.0157	0.0013	2.219	9.71	383.6	0.00058	63.8	16.1	5.957	0.016
G	0.6	1.601	0.0150	0.0008	1.574	13.4	657.2	0.00046	70.8	30.0	5.820	0.011
H	0.7	1.663	0.0151	0.0009	1.816	7.39	579.5	0.00047	67.6	37.7	5.772	0.017
I	0.7	1.536	0.0150	0.0008	1.367	5.79	644.1	0.00047	73.6	43.7	5.800	0.018
J	0.8	1.875	0.0154	0.0001	2.559	8.71	3771	0.0005	59.5	52.7	5.733	0.016

K	0.9	1.984	0.0181	0.0000	2.979	12.9	22183	0.0011	55.5	66.1	5.656	0.015
L	1.0	1.956	0.0205	-0.0001	2.916	7.09	-	0.00164	55.8	73.4	5.606	0.021
M	1.2	2.027	0.0176	0.0006	3.123	9.27	876.5	0.0010	54.3	83.1	5.656	0.019
N	2.0	1.840	0.0169	0.0006	2.288	9.86	913.7	0.00085	63.1	93.3	5.962	0.016
O	4.0	1.257	0.0149	-0.0009	0.5975	6.47	-	0.00046	85.9	100.0	5.532	0.011
Integrated age ± 2σ				n=13		96.4				K_2O=16.18%	5.826	0.015
Plateau ± 2σ		steps K-M		n=3	MSWD=2.21	29.229				30.3	5.644	0.031
Isochron±2σ		steps K-M		n=3	MSWD=2.13		$^{40}Ar/^{36}Ar$=		333±56		5.06	0.84

Italy-3, Adularia, 1.05 mg, J=0.0028255±0.02%, IC=1.00859±0.0017725, NM-290F, Lab#=65666-01, Argus VI

C	0.3	17.92	0.0631	0.0025	56.92	1.090	200.9	0.0090	6.1	0.9	5.65	0.25
D	0.4	4.833	0.0181	0.0002	12.83	1.62	2761	0.00068	21.4	2.2	5.343	0.090
E	0.4	2.438	0.0147	-0.0007	4.518	2.64	-	0.00025	45.0	4.3	5.652	0.047
F	0.5	1.883	0.0140	0.0006	2.703	10.58	826.9	0.00018	57.4	12.8	5.554	0.016
G	0.6	1.507	0.0141	0.0002	1.429	17.2	3028	0.00024	71.8	26.7	5.554	0.009
H	0.7	1.448	0.0137	0.0006	1.210	10.84	812.0	0.00018	75.2	35.4	5.586	0.011
I	0.7	1.458	0.0139	-0.0001	1.261	7.68	-	0.00021	74.3	41.6	5.560	0.014
J	0.8	1.694	0.0141	0.0000	2.039	19.7	-	0.00023	64.2	57.4	5.589	0.010
K	0.9	1.284	0.0137	0.0005	0.6584	16.0	1097	0.0002	84.7	70.3	5.579	0.007
L	1.0	1.184	0.0134	0.0013	0.2936	5.40	394.6	0.00014	92.6	74.6	5.621	0.012
M	1.2	1.504	0.0148	0.0006	1.405	25.3	791.6	0.00041	72.2	95.0	5.579	0.008
N	2.0	1.120	0.0133	0.0015	0.0864	6.20	348.9	0.00013	97.7	100.0	5.609	0.010
Integrated age ± 2σ				n=12		124.2				K_2O=16.07%	5.577	0.011
Plateau ± 2σ		steps C-N		n=12	MSWD=3.92	124.2				100.0	5.582	0.013
Isochron±2σ		steps C-N		n=12	MSWD=3.72		$^{40}Ar/^{36}Ar$=		294.0±1.1		5.592	0.009

Notes:

Isotopic ratios corrected for blank, radioactive decay, and mass discrimination, not corrected for interfering reactions.

Errors quoted for individual analyses include analytical error only, without interfering reaction or J uncertainties.

Integrated age calculated by summing isotopic measurements of all steps.

Integrated age error calculated by quadratically combining errors of isotopic measurements of all steps.
Plateau age is inverse-variance-weighted mean of selected steps.
Plateau age error is inverse-variance-weighted mean error (Taylor, 1982) times root MSWD where MSWD>1.
Plateau error is weighted error of Taylor (1982).
Isochron and error determined using York (1969).
Isotopic abundances after Steiger and Jäger (1977).
X preceding sample ID denotes analyses excluded from plateau age calculations.
i symbol preceding sample ID denotes analyses excluded from isochron age calculations.
– K/Ca not determined as no measureable ^{37}Ar above blank level.
IC = measured $^{40}Ar/^{36}Ar$ of air standard divided by 295.5
Ages calculated relative to FC-2 Fish Canyon Tuff sanidine interlaboratory standard at 28.201 Ma
Decay Constant (LambdaK (total)) = 5.463e-10/a
Correction factors:

$(^{39}Ar/^{37}Ar)_{Ca}$ = 0.00073 ± 0.000020
$(^{36}Ar/^{37}Ar)_{Ca}$ = 0.0002725 ± 0.0000009
$(^{38}Ar/^{39}Ar)_{K}$ = 0.012718 ± 0.00008
$(^{40}Ar/^{39}Ar)_{K}$ = 0.0088 ± 0.0004

Figure 1

Figure 2

Figure 3

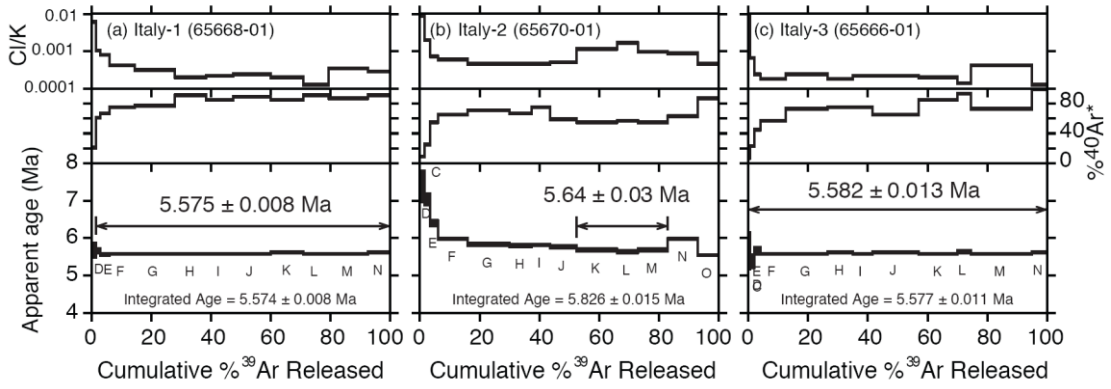
(a) Italy-1 (65668-01)
(b) Italy-2 (65670-01)
(c) Italy-3 (65666-01)
Cl/K
0.01
0.001
0.0001
Apparent age (Ma)
5.575 ± 0.008 Ma
5.64 ± 0.03 Ma
5.582 ± 0.013 Ma
Integrated Age = 5.574 ± 0.008 Ma
Integrated Age = 5.826 ± 0.015 Ma
Integrated Age = 5.577 ± 0.011 Ma
%40Ar*
Cumulative %39Ar Released
Cumulative %39Ar Released
Cumulative %39Ar Released

Figure 4

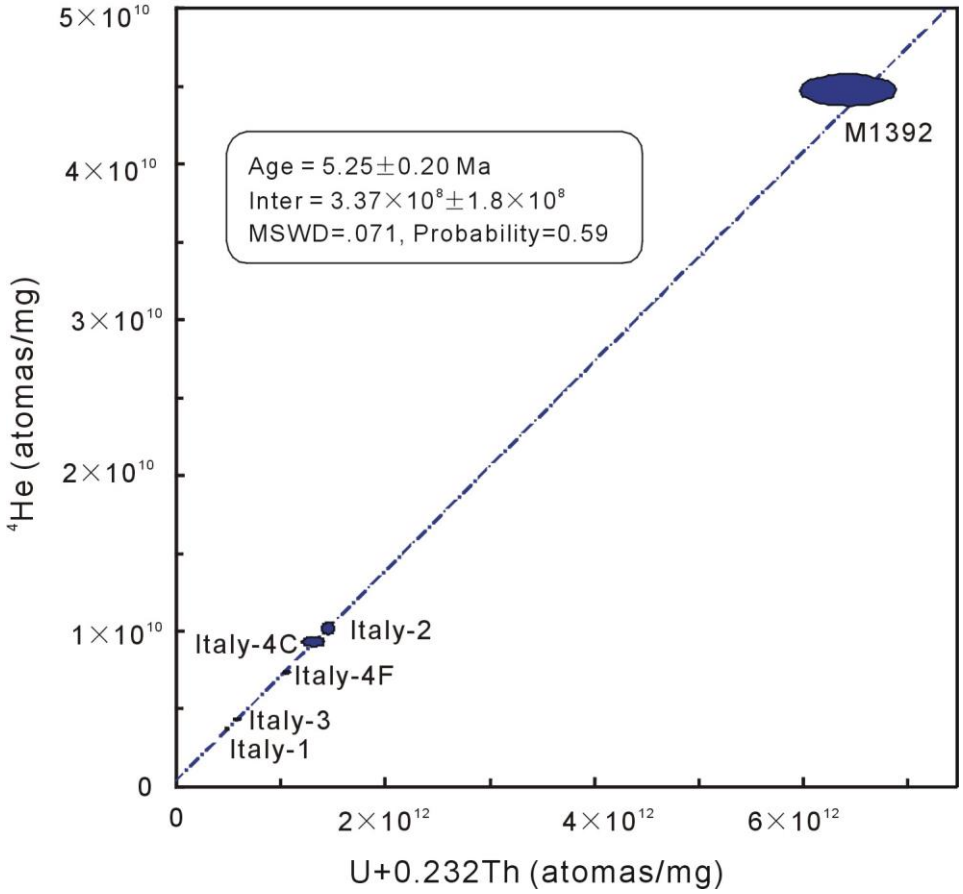
5×10^10
4×10^10
3×10^10
2×10^10
1×10^10
0
4He (atomas/mg)
Age = 5.25±0.20 Ma
Inter = 3.37×10^8±1.8×10^8
MSWD=.071, Probability=0.59
M1392
Italy-4C
Italy-2
Italy-4F
Italy-3
Italy-1
0
2×10^12
4×10^12
6×10^12
U+0.232Th (atomas/mg)

Figure 5